Application of DInSAR Technique to High Coherence Sentinel-1 Images for Dam Monitoring and Result Validation Through *In Situ* Measurements

Silvia Liberata Ullo, Pia Addabbo, Diego Di Martire, Stefania Sica, Nicomino Fiscante,
Luca Cicala, and Cesario Vincenzo Angelino

***Abstract*—Dam monitoring represents a crucial issue in order to avoid catastrophic failures due to infrastructure aging or earthquake damages. Differential SAR Interferometry (DInSAR) is a technique suitable for critical infrastructure monitoring, also for the availability of free data and tools, that can be used by experts in SAR remote sensing and also by geologists and civil engineers, after having acquired the right confidence and experience in these data processing and tool use. In order to apply the DInSAR technique, in its basic and simple version, to critical infrastructure monitoring, it is very important to assess its performance. Nevertheless, validation results are not largely available in literature, because heterogeneous technical competencies are required to this aim and *in situ* measurements must be collected and made available. In this paper, we propose a highly reproducible DInSAR workflow that can be effectively used for dam monitoring, by validating its results with *in situ* measurements on some significant case studies in Italy.**

***Index Terms*—Dam monitoring, Differential Synthetic Aperture Radar Interferometry (DInSAR), geohazard assessment, image coherence, *in situ* measurements, result validation, Sentinel-1.**

I. Introduction

GEOHAZARDS comprise natural geological and environmental phenomena, such as earthquakes, landslides, subsidence, and tsunamis, which may cause devastating effects on populations, territory, and economies. This long-term or short-term process may significantly impact the affected territories on both local and regional scales. Understanding the phenomenon evolution may be a first important step in risk mitigation, such as in the case of slow landslides or subsidence, or in the case of sudden catastrophic events, such as the barrage or auxiliary structure collapse of dams, for instance.

Traditionally, dam monitoring is accomplished by taking under control superficial displacements, measured by geodetic techniques [collimation, high-precision leveling, and Global Positioning System (GPS)]. For earth dams, which from the viewpoint of monitoring strategies [1] are more similar to slopes than to concrete structures, tools such as inclinometers and cross arms are used to detect internal displacements and settlements, respectively [2]. Geotechnical instruments are placed in one or more significant cross Sections of the embankment to ascertain its response in two-dimensional (2-D) or even 3-D, during the whole dam lifetime, including eventual seismic stages [3], [4]. The main shortcoming of the traditional survey is represented by the reduced number of monitoring stations, which cannot assure the desired spatial density in the required information, unless prohibitive operating costs and long data processing. Each typology of traditional *in situ* instruments (piezometers, clinometers, inclinometers, assestimeters, load cells, etc.) is regularly read at time intervals that typically range from one week to a few months, depending on site conditions, age of the dam [5], and stage of the dam lifetime. *In situ* monitoring, for instance, is increased immediately after a strong seismic event to detect eventual behavioral anomalies caused by the earthquake. It should be pointed out that the deformation process interesting a well-designed earth dam or its foundation soils is very slow and appreciable modifications (if any) may span over very long periods, from months to decades. This means that monitoring through traditional instrumentation can be performed only through the collection of a huge amount of data, which must be suitably processed to extract useful information over time. Alternatively, other surveying techniques may be used, which have arrays of targets on the monitoring surface itself. Coordinates of surface points are measured by Electronic Distance Measurement devices, for instance, by means of Total Product Stations (TPSs) and/or GPS devices, allowing an automatic and continuous monitoring. More recent systems can deliver continuous data in almost real time and may be logged to a local computer or transmit directly back to a remote server in the office [2].

To overcome the limitations related to the traditional measurements for dam monitoring, data acquisition from satellites can be effectively used since they allow to cover the area to

Manuscript received June 16, 2018; revised November 4, 2018 and December 5, 2018; accepted January 20, 2019. Date of publication February 28, 2019; date of current version March 25, 2019. *(Corresponding author: Silvia Liberata Ullo.)*

S. Liberata Ullo, S. Sica, and N. Fiscante are with the University of Sannio, Benevento 82100, Italy (e-mail: ullo@unisannio.it; stefsica@unisannio.it; nicomino.fiscante@unisannio.it).

P. Addabbo is with the Giustino Fortunato University, Benevento 82100, Italy (e-mail: p.addabbo@unifortunato.eu).

D. Di Martire is with the University Federico II, Napoli 80138, Italy (e-mail: diego.dimartire@unina.it).

L. Cicala and C. V. Angelino are with the CIRA, Italian Aerospace Research Center, Capua 81043, Italy (e-mail: l.cicala@cira.it; c.angelino@cira.it).

Color versions of one or more of the figures in this paper are available online at http://ieeexplore.ieee.org.

Digital Object Identifier 10.1109/JSTARS.2019.2896989

be monitored, in a spatially distributed manner also over very large time periods. Moreover, it allows the useful combination of data from different sources, by resulting in new promising monitoring geographical tools and systems.

Satellite-borne SAR Interferometry (InSAR) is an emerging technique to monitor dams and several papers in the specific literature revolve around SAR monitoring strategies applied to concrete dams [6]–[8] or earth dams [1], [9]–[13] or both typologies [14]. Some of them are based on Differential SAR Interferometry (DInSAR) processing on distributed scatterers. Worth citing is the case of the Mosul Dam (Iraq) for which SAR measurements [13] allowed to detect an increasing rate of subsidence due to dissolution of wide gypsum strata below the dam basement. In such an extreme case, the possibility of using remote satellite data proved to be effective in difficult operating conditions, in checking the evolution of an already known process (grouting injections were stopped for a while due to temporary control of the dam by the Islamic State to avoid water infiltrating in the soluble materials of the foundation). The Mosul Dam is, however, paradigmatic of extreme conditions a dam could experience in its lifetime as, for example, it could occur after a strong earthquake for those dams built on fault areas [15], [16]. In these conditions, traditional monitoring stations may stop functioning and require some time to be replaced in operation. In this intermediate stage, remote sensing data analysis may prove extremely useful since it becomes the unique source of information on dam and reservoir stability, when field measurements are temporary unmanageable. Sometimes more than one interferometric method was adopted to improve the precision level required to monitor the small deformations of dams, especially for concrete dams, typically founded on highly stable basins (rock), less prone to vertical displacements. In this case, dam movements are mainly horizontal, since linked to temperature changes and oscillations of the water impounding for hydroelectric use. To detect, for instance, the main factors contributing to the Three Georges Dam (China) deformation, after its completion, in [6], authors proposed to combine two different interferometric methods, the PS (Permanent scatterer) and quasi-PS techniques. As expected, the consolidation settlements of the dam foundation, made of granite, were found to be negligible, while wide areas of subsidence were found far from the dam along the reservoir slopes. Yet, with respect to classic DInSAR methods, based on distributed scatterers, the PS approach limits the analysis to a few high-coherence points. However, to have a reliable analysis, a sufficient number of PSs should cover the monitored structures [17]. Since, in general, the lower is the SAR wavelength, the higher is the number of PSs, this approach may not be the best to adopt for high-frequency satellite data. In [1], a protocol to acquire and process Ground-Based SAR (GB-SAR) and Real Aperture Radar measurements for earth dam monitoring was presented. The advantages of using two GB-SAR systems, properly located with respect to the dam, were to provide a more effective visualization and quantitative analysis of dam displacement. Yet, as underlined before, the advantage of satellite data in dam safety monitoring systems relies on their availability also in adverse conditions, and on their capacity to provide early warning when behavior anomalies occur.

In this paper, a DInSAR processing workflow based on free ESA data (Sentinel-1) and tools [Sentinel Application Platform (SNAP)] is proposed for dam monitoring. The results, obtained on significant case studies in Italy, are validated comparing them with *in situ* measurements. By discussing significant case studies, we assess the performance of the proposed high reproducible DInSAR approach and, with the obtained satisfying results, we show the effectiveness of SAR interferometry for the specific application, in order to complement or substitute (when needed) *in situ* measurements.

It is worth to highlight that even if result validation is crucial for the success of dam monitoring application through DInSAR, it is not broadly available in literature, mainly due to lack of *in situ* data and need of interdisciplinary competences for their analysis (among the cited papers dealing with satellite dam monitoring, only [10] and [11] include validation results).

Furthermore, the encoded procedures have been provided results that may be easily extended also to monitoring different types of infrastructures, with the final aim of risk mitigation. Such results, accurately validated, support the feasibility of dedicated monitoring services, based on data combination from different sources: remote sensing satellite data and *in situ* measurements.

The paper is organized as follows. Section II will briefly summarize main aspects of remote sensing and present the Copernicus Programme and Sentinel-1 mission and characteristics. Section III will introduce the chosen technique, the DInSAR, presenting its main applications within the geohazard area of interest. In this section, some aspects that appear to be critical in order to achieve good interferograms are analyzed. The workflow of the Sentinel-1 SNAP tool for data processing and interferogram generation is also presented, emphasizing its criticality as topics of discussion. In Section IV, the case studies will be illustrated and data of the *in situ* monitoring presented. Section V will show and discuss data processing and results, while final comments and proposals for future developments are highlighted in Section VI.

II. Copernicus Programme and the Sentinel-1 Mission

The proposed approach is based on free remote sensing data and processing tools from the European Copernicus programme [18], [19] and aims at developing geographical information services for environmental monitoring based on satellite remote sensing and *in situ* measurements.

Sentinel satellites, when specific acquisition tasks are not committed, are employed in a default continuous Earth coverage programme, in order to build an updated large global archive. Sentinel datasets are freely available online through the Open Access Hub (previously known as Sentinels Scientific Data Hub). The provided images can be processed not only through commercial professional tools but also by dedicated freely downloaded software, distributed by ESA [20] and based on a common architecture framework, named SNAP [21].

Regarding Sentinel-1, to which we are interested for the purpose of our work, the main features concern the acquisition modes (summarized in Fig. 1) [22]: StripMap mode,

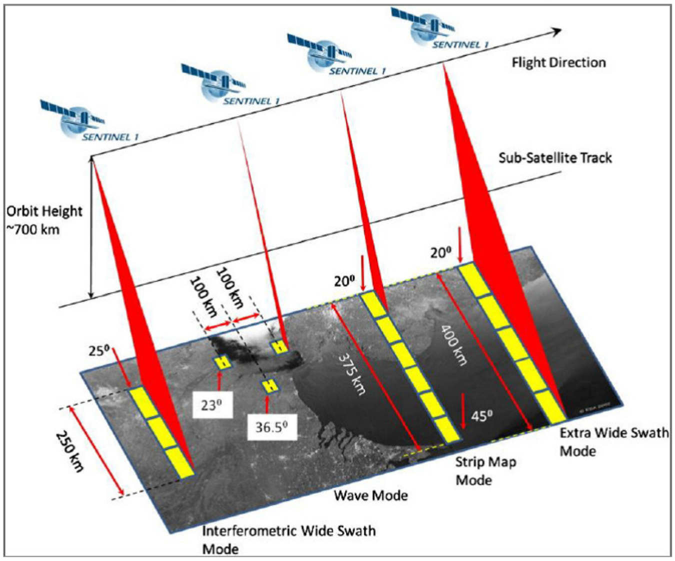

Fig. 1. Sentinel-1 acquisition modes (Courtesy of ESA).

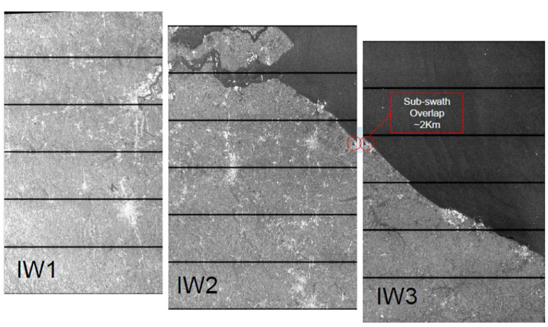

Fig. 2. Images belonging to the same Sentinel-1 IW product bundle: subswaths and bursts (Courtesy of ESA).

Interferometric Wide (IW) swath mode, Extra Wide swath mode, and Wave Mode.

IW is the default acquisition mode over land. It captures three subswaths using the Terrain Observation with a Progressive scans SAR (TOPSAR) technique, that steers the beam both in range and in azimuth, for each burst. IW products contain one image per subswath and one per polarization channel, in practice three (single polarization) or six (dual polarization) images. Each subswath image consists of a series of bursts, each of them processed as a single image. These bursts are composed in a single subswath image with black fill demarcation in between. A small overlap among adjacent bursts provides contiguous coverage of the ground. It is worth to notice that all the bursts can be resampled to a common pixel space, preserving phase information. Fig. 2 shows images belonging to the same Sentinel-1 IW product bundle, divided into subswaths and bursts.

Sentinel-1 data products are distributed at three levels of processing [22]: Level-0 (compressed and unfocused data), Level-1 [focused data, Single Look Complex (SLC), or Ground Range Detected], and Level-2 (processed data, like Ocean Wind field, Ocean Swell spectra, and Surface Radial Velocity).

The Sentinel-1 data used in the paper are Level-1 SLC images acquired through the IW mode. Data processing has been performed using the SNAP Toolbox that includes specific packages for SAR calibration, speckle filtering, coregistration, geocoding, mosaicking, polarimetry, and interferometry. It is worth to highlight that the use of the SNAP toolbox is not straightforward, but it requires familiarity with remote sensing principles and, in particular, with SAR processing chains. One of the aims of this paper is to stimulate and support interested readers in developing monitoring approaches, based on using available SAR data and processing software from the Copernicus programme. Moreover, dissemination of this paper results, obtained on significant case studies, is expected to contribute positively to the proposition of novel Copernicus services, for dam monitoring and in general for other strategic infrastructure monitoring, based on multitemporal SAR interferometry.

III. Differential SAR Interferometry (DInSAR)

Among the different types of remote sensing techniques, one that very well meets requirements for dynamic process analysis is the DInSAR [23]. DInSAR is the method used to process SAR generated images and it is based on the combination of one or more pairs of satellite images whose orbital parameters are all known. The combination of two SAR images of the same scene, acquired from slightly different orbits produces the interferogram. As shown in Fig. 3, it is obtained by multiplying one image by the complex conjugate of the other and contains, on a pixel by pixel basis, the phase difference between the two acquisitions [24]. For each acquisition, this phase difference can be exploited in combination with the orbital information, in order to derive a Digital Elevation Model (DEM) of the scene. If this latter is known, the DInSAR technique allows calculating the terrain displacements, since the interferometric phase contains the following phase term:

$$\Delta\phi_d = \frac{4\pi}{\lambda}\Delta R \quad (1)$$

with ΔR the projection of the relative point displacement onto the radar Line of Sight (LOS).

In an ideal configuration, the DInSAR technique allows to get measurements of the LOS displacement of the order of wavelength fractions, provided that the coherence among the two different images is sufficiently high. Indeed, an LOS displacement of $\lambda/2$ results in a differential phase change of 2π. Since the error in the phase estimate is of a fraction of π and the wavelength is of the order of centimeters (e.g., for the Sentinel-1 case $\lambda = 5.5$ cm), LOS displacement down to millimeter accuracy can be measured. However, in real cases, the differential interferograms contain some unwanted phase terms due to the nonperfect knowledge of topography and/or the orbital parameters. In particular, the variation of the interferometric phase can be expressed more in general in the form

$$\Delta\phi = \Delta\phi_d + \Delta\phi_{\text{topo}} + \Delta\phi_{\text{orb}} + \Delta\phi_{\text{atm}} + \Delta\phi_n \quad (2)$$

where the following conditions hold.

1) $\Delta\phi_d$ accounts for a possible displacement of the scatterer between observations.

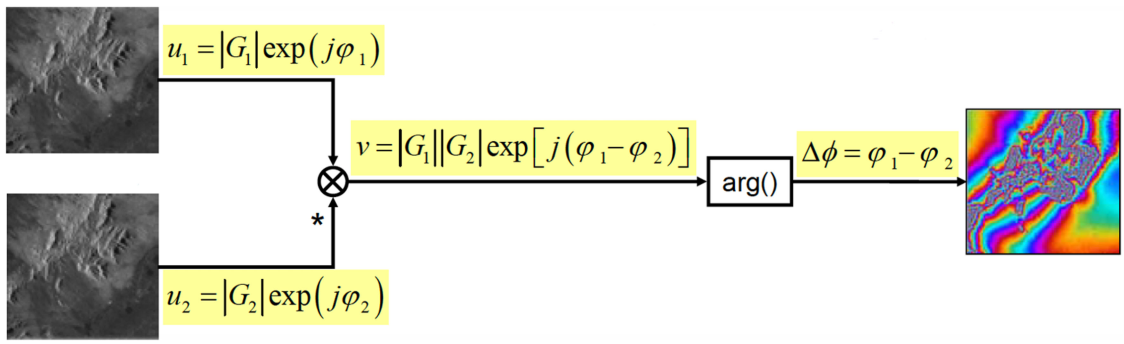

Fig. 3. Interferogram is generated by multiplying two (complex) SAR images and then extracting the phase (Courtesy of ESA).

2) $\Delta\phi_{\text{topo}}$ represents the residual topography induced phase due to a nonperfect knowledge of the actual height profile (i.e., the DEM errors).
3) $\Delta\phi_{\text{orb}}$ accounts inaccurate orbital information in the synthesis of the topographic phase.
4) $\Delta\phi_{\text{atm}}$ denotes the phase components due to the change in the atmospheric and ionospheric dielectric constant between the two master/slave acquisitions.
5) $\Delta\phi_n$ accounts for decorrelation phenomena (spatial, temporal, thermal, etc.).

In the following, some fundamental steps and critical aspects of interferometric processing are analyzed.

A. Image Coregistration

Coregistration performs the alignment of the SAR images so that they could be compared pixelwise for differences. The standard Sentinel-1 TOPS acquisition mode requires a coregistration accuracy of 0.001 pixel in order to avoid introducing nonnegligible phase error into the interferogram. The suggested Sentinel-1 coregistration processing workflow performs a first step based on back geocoding, followed by a further registration method called Enhanced Spectral Diversity (ESD). The back-geocoding approach could be seen as a mapping from SAR coordinates to Cartesian coordinates with the help of very precise orbits and DEM. The coregistration accuracy for this approach mainly depends on the accuracy of orbital state vectors. With the availability of precise orbital state vectors for Sentinel-1 with an accuracy of 5 cm, this approach is suitable as initial coregistration method. After that, the ESD method is applied to correct the residual coregistration error and achieve the coregistration requirement for TOPS. ESD compares the phase differences of two images and the azimuth miscoregistration is derived from this differential phase.

B. Coherence Issues

As underlined in the previous section, the coherence among images represents a very critical issue since only high-coherence images result in a reliable interferogram. A measure of how much the two images are comparable, pixels by pixel, is given by

$$\gamma = \frac{E[u_1 u_2^*]}{\sqrt{E[u_1 u_1^*]E[u_2 u_2^*]}} \tag{3}$$

where $E[\cdot]$ denotes statistical expectation, u_1 and u_2 represent the two images. The coefficient values from (3) range from 0 (low coherence) to 1 (high coherence). Coherence, or better its modulus (since it is a complex quantity), provides a useful measure of the reliability of the result. Indeed higher values of coherence correspond to lower contribution of the interferometric noise. From literature, images with coherence higher than $0.35/0.4$ lead to good results [25], [26].

The image coherence, when an interferogram must be calculated, has an important diagnostic function. Excluding random noise, the loss of coherence is mainly caused by geometrical and temporal decorrelations. While the former depends on the acquisition geometry and can be controlled by choosing a proper baseline, the latter depends also on the scattering properties of a target [27]. For example, water bodies have very low coherence because their surfaces are constantly moving; they, therefore, appear black in coherence images. Vegetation usually presents low coherence because of several reasons, such as, the volume scattering, the water content, the leaf motion, the vegetation growth, etc. However, it depends on the wavelength. Indeed, if this holds for X-band (or C-band) SAR systems, where the radiation can only reach the top of the canopy, for L-band (or P-band), the radiation can generally penetrate the canopy and can be backscattered by the terrain underneath or by the trunk and the branches of the trees. On the contrary, rocks, buildings, roads, and artificial constructions present generally a high coherence.

High-coherence values are fundamentals for the phase unwrapping step. Unfortunately, SAR interferometric surveys are affected by several sources of decorrelation noise. An improvement of the phase accuracy can be achieved by minimizing that noise and this requires specific processing. The techniques used to minimize the effect of different decorrelation sources will be in detail explained in the workflow showing the SNAP steps.

Fig. 4 shows two examples of interferograms: one from low-coherence images and one from high-coherence images.

C. Phase Unwrapping for DInSAR Application

One of the most challenging aspects in the successful application of DInSAR technique is unwrapping the interferometric phase [28]–[30]. The difficulties arise in attempting to find global optimization procedures with the best possible cost criteria for data that are both noisy and incomplete. The

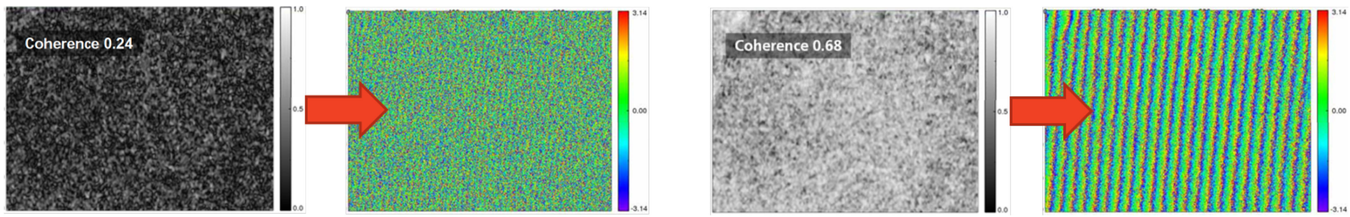

Fig. 4. Examples of Interferograms from low-coherence and high-coherence images (Courtesy of ESA).

absolute unwrapped interferometric phase is directly proportional to the difference in path lengths for the SAR image pair. Interferometry applications link the unwrapped phase to geophysical parameters, such as elevation and deformation, due for instance to ice motion, surface subsidence, earthquakes, volcanic inflation/deflation, and tectonic motion. The complex-valued interferograms, however, present an ambiguity exactly corresponding to multiples of 2π and must be unwrapped to obtain a quantitative interpretation. Phase unwrapping is the process of restoring the correct multiple of 2π to each point of the interferometric phase image. For a well-behaved smooth phase field, all the unwrapped phase differences between adjacent interferogram samples lie between $-\pi$ and $+\pi$. When this is true, phase unwrapping is straightforward since the unwrapped phase can be evaluated by a simple (path-independent) integration of the phase differences of adjacent wrapped phases, starting from a reference location and using the assumption that all phase differences are in the interval $(-\pi, +\pi)$. In actual interferograms, however, phase unwrapping is more complicated because the unwrapped phase differences, between adjacent interferogram samples, lie outside the interval $(-\pi, +\pi)$.

D. Data Processing Workflow

The Sentinel-1 data processing is performed through the SNAP software platform, published under the GPL-3 license by ESA, for EO processing and analysis [31]. One of the key aspects of SNAP is its modular architecture that allows users to create appropriate workflows. Specifically, in order to generate a displacement map on the site of interest, a data processing chain, made by different and consecutive steps, is implemented in SNAP (Fig. 5). The entire workflow can be divided into three main Sections.

The first main section is the preunwrapping step, where starting from a pair of (master and slave) images, downloaded from the ESA site and imported into the SNAP environment, a series of substeps are performed. TOPSAR coregistration step is useful to split out the different subswaths, with the relative selected bursts, in separate products and to select the type of polarization. Coregistration is a necessary step to match the same points on the earth surface in different images and a very stringent accuracy is needed in this case. Usually, a split operation on both master and slave image is required together with an orbit correction, where the split operation consists into the selection of single subswaths from the whole initial burst in each image, accomplished inside the TOPSAR coregistration step, through the TOPSAR-split substep. After the TOPSAR coregistration,

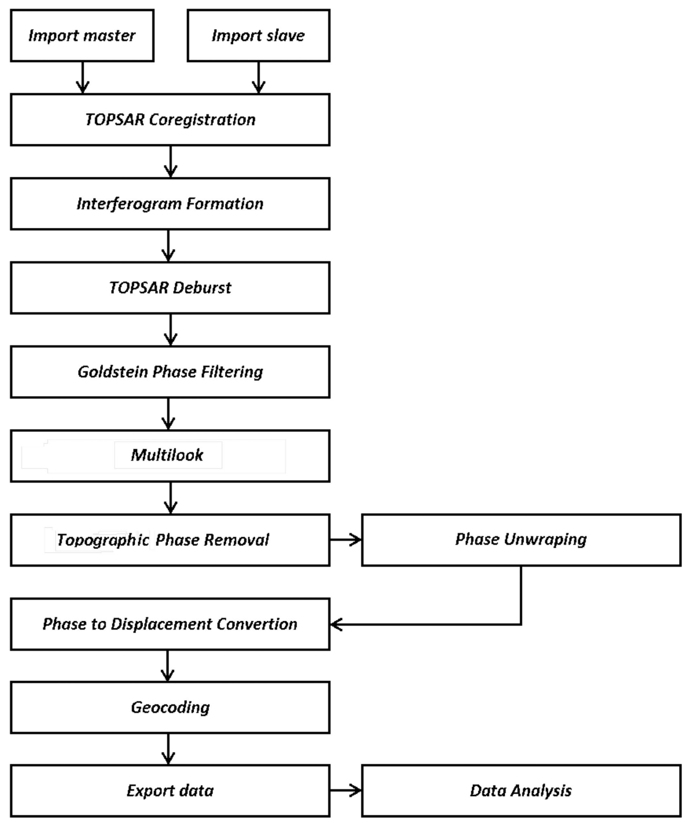

Fig. 5. Workflow implemented in SNAP for the displacement map generation.

the Interferogram Formation step is carried on, where it may be useful the flat-earth phase elimination to improve the further steps. The flat-earth phase is included in the interferometric signal and is due to earth curvature. If the two orbits needed for interferometry are known, the flat-earth phase is estimated using the available orbital information and metadata, and is then subtracted from the complex interferogram. The Deburst step is necessary to merge the burst related to the area of interest. Usually to reduce the subsequent processing time, the Subset operator is also used to extract a portion of the image. Among all these steps, the application to the interferogram of the multilooking and the phase filtering operations is very important to obtain optimal results in the subsequent phase unwrapping step. Multilooking is used to reduce Speckle noise and phase filtering (usually performed through a Goldstein filter) to then improve accuracy during unwrapping step. The preunwrapping step ends with the topographic phase removal.

The removal of the topographic phase component is not accomplished when a DEM must be generated, but for this please refer to the specific paragraph in Section V, Data Processing and Results.

The second main section is the phase unwrapping step performed through SNAPHU, a Statistical-cost Network-flow Algorithm for phase unwrapping developed at Stanford University [32]. SNAP contains the import–export functions for the external data processing in SNAPHU. 2-D phase unwrapping is the process of recovering unambiguous phase data from a 2-D array of phase values, once that only modulus 2π is known. The SNAPHU algorithm poses phase unwrapping as a maximum *a posteriori* estimation problem, the objective of which is to compute the most likely unwrapped solution given the observable input data. Because the statistics linking the input data to the solution depend on the measured quantity, SNAPHU incorporates three built-in statistical models, for topography data, deformation data, and smooth generic data. The optimization problem is solved approximately with the use of network-flow techniques. SNAPHU produces reliable unwrapped solutions, depending on the input interferogram, and its accuracy is comparable to other available algorithms. As SNAPHU uses an iterative optimization procedure, its execution time depends on the difficulty of the interferogram [33]–[35]. The quality and reliability of unwrapped results, as already underlined, strongly depends on the input coherence of the images. Reliable results can only be expected in areas with high coherence, although a "phase continuity assumption" is also necessary so that unwrapping can work correctly. Explicitly the phase continuity assumption requires the absolute phase difference between any adjacent pixels be less than π radians in magnitude [36].

The third main section is the postunwrapping section, where the unwrapped phase is directly converted into a displacement because the topographic contribution to the interferometric phase has been already removed within the preunwrapping steps. It is worth noting that, in real applications, the unwrapped phase may still contain residuals from the removal of the DEM phase because of topography errors. The phase to displacement operator generates the displacement values in accordance with (1). The calculation of these displacements is performed along the LOS of the remote sensing system. To obtain the vertical displacements, it is necessary to know the incident angle and multiply the calculated displacements times the LOS-vertical factor, assuming only vertical displacement. After that, a range doppler orthorectification for geocoding the data must also be applied [37]. Finally, the georeferenced displacement map can be exported to different formats and used within a GIS application, such as Google Earth.

IV. Case-Study Reservoirs

The present paper is focused on two large reservoirs in Italy: the Campolattaro and the Campotosto reservoirs. In the first case, the reservoir is made by a unique earth dam obstructing the river Tammaro; in the second case, the reservoir is formed by three dams, two of which are of concrete typology (Rio Fucino and Sella Pedicate), while the third one (Poggio Cancelli) is an earth dam. In Fig. 6, the Campolattaro and the Campotosto reservoirs are shown on the left and on the right, respectively.

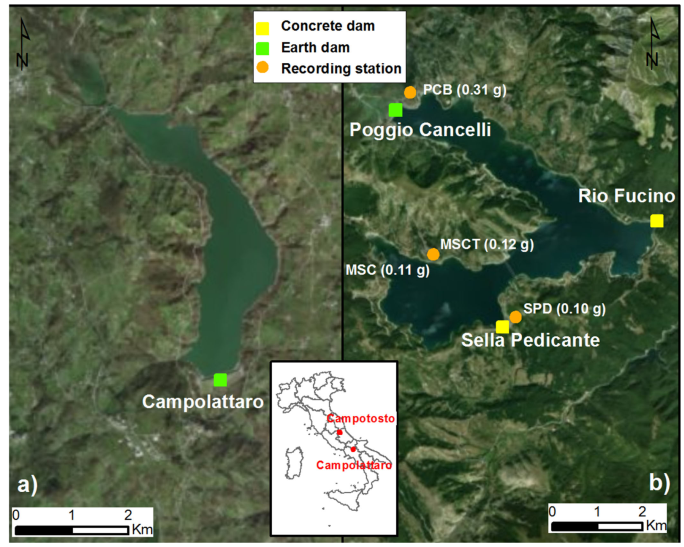

Fig. 6. Maps showing the Campolattaro and Campotosto reservoirs, on the left and on the right, respectively: in the frame, the exact locations of the dams are reported over Italy.

A. Campolattaro Reservoir

The Campolattaro dam is placed in Benevento, which is one of the most seismic areas in Southern Italy. The embankment was built between 1986 and 1992. The maximum water storage of the reservoir is of about 125 millions of m^3. The geometrical features of the dam embankment are the following:

1) Crest elevation: 387.40-m a.s.l. (above sea level);
2) Crest width: 9 m;
3) Length of the crest: 820.60 m;
4) Maximum embankment height: 62.90 m.

The geotechnical characterization of the foundation and dam soils are based on the results of two recent investigations, carried out in 2009 and 2016. The dam core is made of low-plasticity clayey silt with sand; the shells and the drains are made of gravels with sand, while the foundation soils consist of silty clayey sandstone dating back to the Miocenic Age.

The dam is under the control of the "Agenzia Sannita Energia Ambiente" ASEA (an agency of the Benevento Province), that has its technical and economic management [39]. The dam is in the stage of the trial fillings, i.e., it is subjected to filling and emptying at predetermined time cycles to monitor its response before the achievement of the maximum storage capacity. Settlements of the dam embankment are measured by means of assestimeters placed in different vertical lines within the dam body. The system consists of a probe, connected to a measuring cable, and a number of spider magnets positioned along a guide tube that crosses the earth embankment. Several magnets are placed in the guide tube at different depths. The first sensor is generally at the head of the guide tube. The magnets follow soil displacements. Reading is obtained by inserting the probe into the guide tube until it finds one magnet, and the depth of

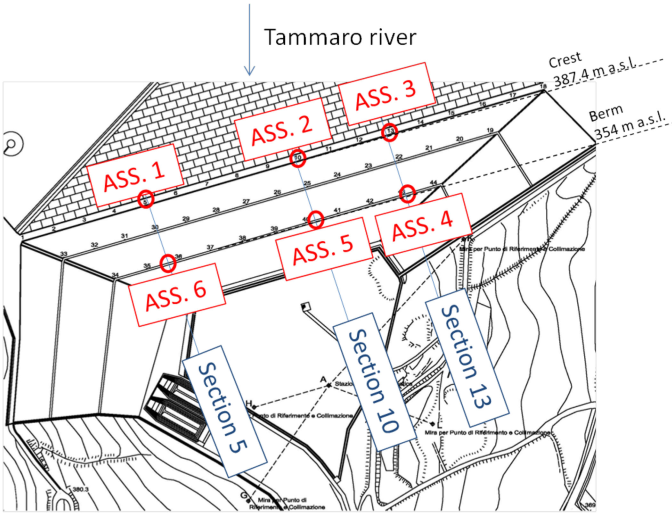

Fig. 7. Position of the assestimeters (red circles) and high-precision leveling targets (numbers) for the Campolattaro dam.

interception can be read from the probe. It is worth noting that in this type of instrument the value 0 of the measurement corresponds to the first time the sensors have been mounted and read, so the displacement is always calculated relatively to the initial configuration of the guide tube.

As shown in Fig. 7, six assestimeters are mounted on the Campolattaro dam: three positioned along the crest and three along the intermediate berm. The assestimeters are placed in three different cross Sections of the embankment (Sections 5, 10, and 13), in such a way to compare vertical displacements along the same section in at least two different points of the structure. For the sake of clarity, the whole assestimeter configuration is the following: Assestimeter 1 and 6 at Section 5, Assestimeters 2 and 5 at Section 10, and Assestimeters 3 and 4 at Section 13. The Assestimeter 1 has 11 sensors, the Assestimeter 2 and 3 have 14 sensors, and the Assestimeters 4, 5, and 6 have 6 sensors. The recorded ground data are available from May 2009 up to January 2017 (data kindly provided by the Province of Benevento).

Vertical and horizontal displacements of the dam boundary are also measured by high-precision leveling through several target points, as shown in Fig. 7.

B. Campotosto Reservoir

Campotosto lake, located within the Province of L'Aquila among the municipalities of Campotosto, Capitignano, and L'Aquila, is a man-made water reservoir with a capacity of 300 millions of m^3. It is impounded by three dams: Poggio Cancelli, Sella Pedicate, and Rio Fucino, and is one of the largest reservoir in Europe. Reservoir filling was completed in the 1970's and its water is used for electric power production. Located in one of the most seismically active area of Italy, in the last ten years the Campotosto site has been affected by different seismic events of higher magnitude (e.g., Abruzzo earthquake of 2009 with moment magnitude Mw $= 6.1$ and the recent 2016–2017 Central Italy seismic sequence with Mw reaching the value of 6.5 on October 30, 2016).

The key features of the three dams are recalled from the GEER Report (2016) [38] and summarized hereinafter.

Poggio Cancelli, whose photo of the embankment is shown in Fig. 8 on the left, is an earth dam crossing the Rio Castellano, a tributary of Tronto river. The dam is located about 18 km from the epicenter of the mainshock that occurred on August 24th, 2016, in Italy, in Abruzzo Region. The embankment is 27.5-m high (crest elevation at 1327.5-m a.s.l.) and 600-m long. The dam is composed of a central core, with sand filters and shells. The core is composed of clayey silt; the upstream shell is formed by calcareous material, whereas the downstream shell can be subdivided into two zones, the upper one made of arenaceous material and the lower one of calcareous material. The foundation soils are characterized by coarse-grained alluvial sands and gravels with lenses of fine-grained soils, superimposed on the arenaceous bedrock. The Poggio Cancelli dam is monitored by a complex ground system which includes several control points, located at the crest, within the core and beneath the base of the dam, where settlements and pore pressure are measured. By combining the measurements provided by assestimeters and from collimation, the system allows obtaining separately the settlements of the core and those in the foundation soils. In the immediate aftermath of the August 24th, 2016 earthquake, few millimeters in terms of settlements at the crest of the dam were measured, as after April 6th, 2009 when the other devastating earthquake affected L'Aquila. The Poggio Cancelli dam hosts the PCB station, which, during the August 24th earthquake, recorded a peak ground acceleration (horizontal component) of about 0.31 g. Despite the severity of ground motion, the seismic response of Poggio Cancelli dam was very satisfactory at that date.

Sella Pedicate dam, 20.75-m tall and 750-m long, over most of its length is a concrete dam, while at one of its extremities it is an embankment with a clayey central core and a concrete foundation diaphragm. Fig. 8 (at the center) shows a photo of the concrete dam. The upstream face is very steep, while the downstream face has a much gentle inclination. The dam was built from 1965 to 1971. During the August 24th earthquake, the SPD station recorded a peak ground acceleration of about 0.11 g, and even in this case, the response to the seismic event was satisfactory.

Rio Fucino, the third dam enclosing the Campotosto reservoir on the eastern side, is a concrete gravity dam, with an almost triangular cross section and a straight longitudinal axis, as shown in Fig. 8 on the right. The maximum height of the dam is 49 m (crest elevation at 1327.5-m a.s.l.; deepest foundation level at 1278.5-m a.s.l.) and the length of the crest is equal to 154 mm. The body of the dam is subdivided into 12 ashlars through 11 joints located along vertical planes. An alternating stratification of sandstone and marlstone constitutes the foundation substratum. The Rio Fucino dam is located in the proximity of the Campotosto fault, also known as Fault of Monti della Laga [40]. After both the 2009 L'Aquila earthquake [41] and the 2016–2017 Central Italy seismic sequence [38], no

Fig. 8. Photos of the embankment of Poggio Cancelli (left), Sella Pedicate (center), and Rio Fucino (right) (GEER report, 2016 [38]).

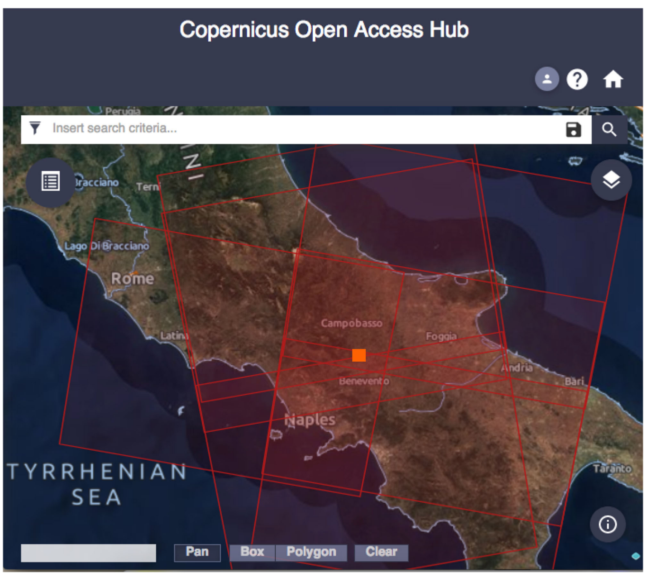

Fig. 9. Position of the area under observation (indicated with an orange small square) with respect to the Sentinel-1 acquisition swaths (represented with great transparent red squares).

significant damage was observed by the ENEL staff on the Rio Fucino dam.

V. Data Processing and Results

As mentioned before, the aim of this paper is to validate the DInSAR results from Sentinel-1 data with on-site measurements in order to demonstrate the feasibility of integrated approaches that can improve the monitoring process of dams as well as of their surrounding areas, mainly in terms of number and location of the observed measurement points.

A. Campolattaro Case Study

The first case study concerns the Campolattaro dam for which a DEM was first generated through a high-coherence interferometric pair. Then, some differential interferograms were generated and the relative displacements derived.

The area surrounding the lake is shown in Fig. 9, with a small orange spot, to highlight how the dam is in a critical point for the choice of the images to be used, since it is in the intersection of three different acquisition orbits, corresponding to different acquisition swaths. This means that although images for the same area are frequently acquired, it is difficult to find two Sentinel-1 products with a small time distance, acquired along the same orbit and that are captured inside the same swath, because it may happen that the two images have been acquired in adjacent subswaths, next to or previous the other one [42]. On the contrary, to proceed with the TOPS coregistration of the images, they must be acquired on the same orbit and belong to the same swath, even if acquired at different time periods. Furthermore, in order to obtain reliable interferometric results, the SAR images have to be chosen with a proper baseline [25]. Given that there is not an optimum baseline, additional considerations must be done to accomplish the baseline choice. In particular, for DEM generation, following conditions should be noticed.

1) Interferograms with a very small perpendicular baseline (<30 m) though easy to unwrap, are almost useless due to their high sensitivity to phase noise and atmospheric effects [27], [28].
2) About atmospheric artifact, characterizing SAR interferograms as a limiting factor, it is important to note that limiting the analysis to small areas, as in our case in which we consider just the dam body, they are negligible and can be considered as a constant phase screen.
3) Interferograms with a large baseline (>450 m) are virtually impossible to unwrap without *a priori* available DEM and if the surface is not uniform; even in the case of *a priori* available DEM and with a flat surface, which allows to completely eliminate the topographic and geometric contribution from the interferometric phase, such a basic line causes low consistency problems due to volumetric scattering and geometric declination, which increase the noise phase up to make the data unreliable [43]–[45].
4) The coherence values are affected by local weather conditions, such as rain, snow, and strong winds, that can cause phase coherence loss and moreover night-time acquisitions are generally less affected by atmospheric effects, while the images in particularly hot days are to be avoided because the hot air contains much more steam than the cold air [46].

1) Generation of DEM From High-Coherence Interferometric Images: For DEM generation, the images must have a small temporal difference and a greater overall coherence. The two

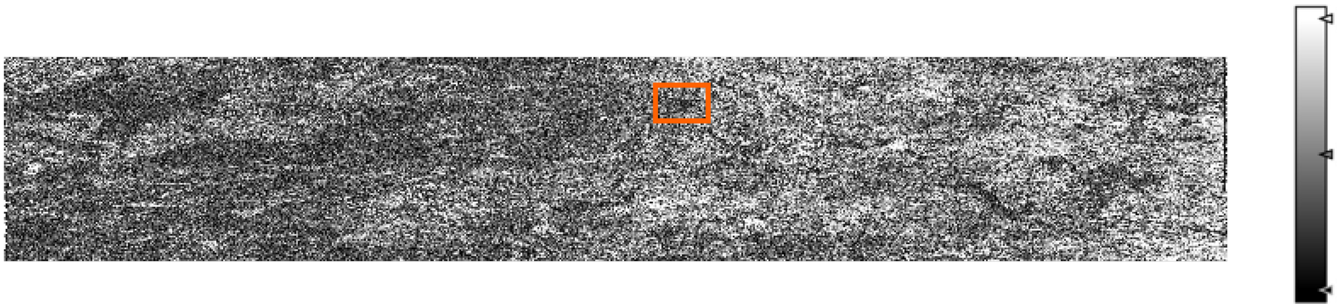

Fig. 10. Coherence of selected Sentinel-1A and Sentinel-1B images acquired, respectively, on November 14th, 2016 and November 8th, 2016. The orange rectangle indicates the subset of the dam under test (see Fig. 11).

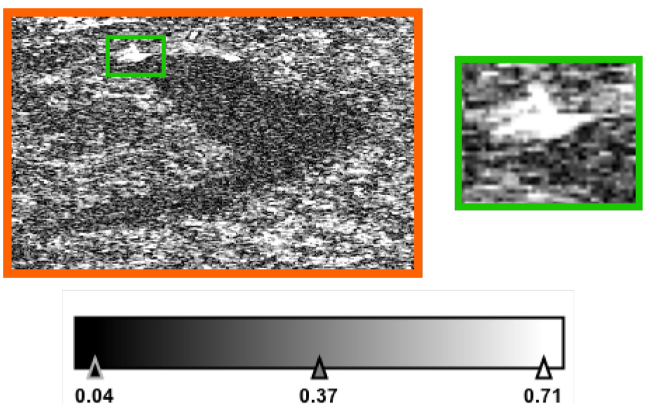

Fig. 11. On the left, the coherence for the subset of the image represented in Fig. 10 and, on the right, the zoomed portion (green rectangle) with the dam body pixels.

images, selected in this case, are one by Sentinel-1B, acquired on November 8th, 2016 and one by Sentinel-1A, acquired on November 14th, 2016, because they have an acceptable perpendicular baseline (116.48 m). The area under observation falls in the second subswath, IW2, for both images, and a VV polarization is used. The high coherence of the selected images is clearly visible in Fig. 10.

From the entire image, a subset is derived to consider only the dam and the nearby area. Fig. 11, on the left, shows the coherence of the image subset and on the right a zoomed portion of this subset with the dam body pixels. The number of pixels with a coherence greater than 0.35 (the value considered as the lowest extremity below which the results are no longer reliable because the phase noise is predominant) is about 44.9%, that means that overall the image presents an acceptable coherence value, that however is not so high and this can be easily explained because the image refers to an area that also contains the water reservoir.

To further improve accuracy, the obtained interferogram must be filtered before the unwrapping. The Goldstein phase filter parameters used are as follows.

1) The adaptive filter exponent is set equal to 1.0.
2) The FFT size, the number of points on which the Fourier discrete transformation is evaluated, is 64.
3) The window size is set to 3.
4) The coherence threshold is 0.2.

It is worth noting that the number of points on which the Fourier discrete transformation is evaluated can be raised, to lower the speckle noise and improve the final result. Yet, this implies increasing the computational load and in addition, if the starting selected subset is too small, the risk increasing the number of points to calculate the FFT is a degradation of the final image instead of improving it [47], [48]. It is worth to say that to generate a DEM, ground control points (GCPs) are necessary because phase measurements are relative. Yet, when the SNAP tool is used, such as in the case we are referring to for Sentinel-1 images processing, the GCPs could be inserted and embedded in the metadata. Then, everything is inside SNAP and in this case we only need to use the necessary operator for the specific product. What we need to do is not removing the topographic component from the interferogram phase, as it is usually done through the "topographic phase removal" operator, because it is exactly that component which defines the ground height necessary for the DEM creation. To execute the height calculation, it is necessary to change the export settings of the phase image in the SNAP tool, because the image must be unwrapped using the SNAPHU tool, and the "statistical-cost mode" parameter must be set to TOPO (topographic) [49].

From the coherence image, we get the pixel coordinates from which to extrapolate the height values for the final DEM provided by SNAP, which is used as a general topographic reference, as shown in Fig. 12, on the left.

Using the SNAP "Profiler Plot" tool, it is possible to draw a broken line along the dam profile, generating the pixel elevation graph, as shown in Fig. 12, on the right. It can be seen that the height of the dam body is between 386 and 389 m and rises at the end for the presence of a hill to the left of the structure. The results are in agreement with the technical data provided by the ASEA handler, listed before, where the crest plate was 387.40-m a.s.l.

Through the Sentinel data acquisitions, the 3-D model of the entire reservoir is generated by the pair of satellite images after correcting the low-coherence pixels, as shown in Fig. 13 on the top. The 3-D model has been generated through a Q-GIS open-source software external to SNAP. The 3-D model of the dam body has also been generated for the zoomed area shown on the right of Fig. 11 through a smoothing process to flat the spikes generated by low-coherent pixels in the DEM, which may still be present over the structure. This 3-D model is shown in Fig. 13 on the bottom.

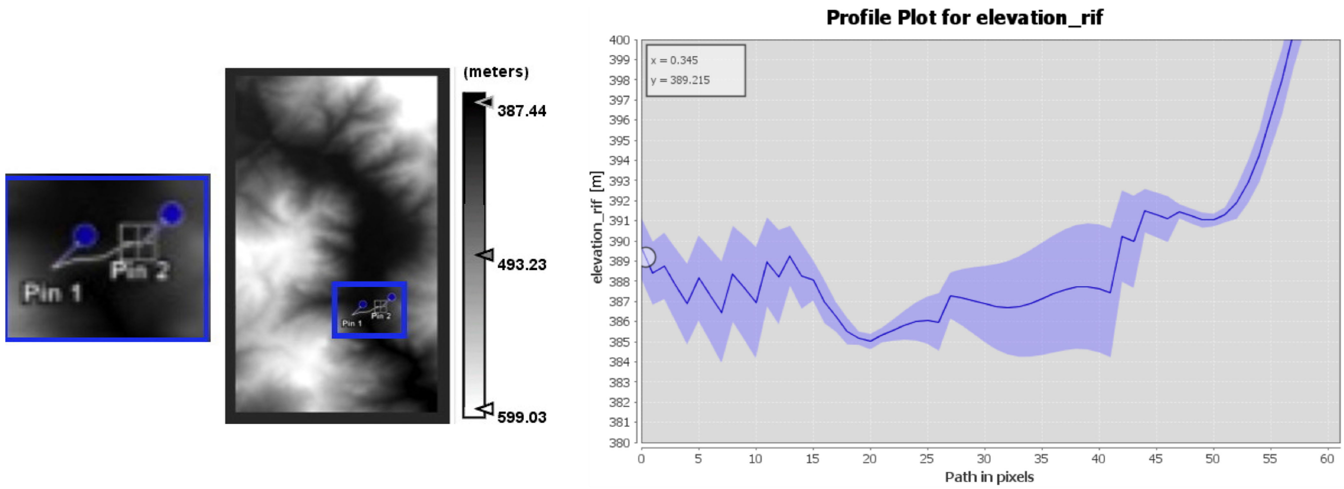

Fig. 12. DEM provided by SNAP used as a general topographic reference with a zoom (blue rectangle) in the area for the profiling pins selection (on the left) and the generated dam elevation profile in meters (on the right).

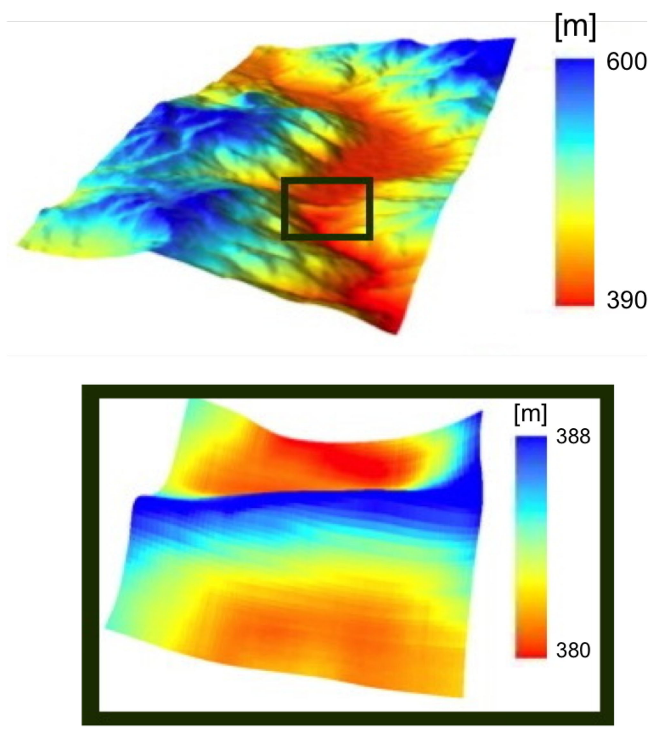

Fig. 13. 3-D digital elevation model of the entire reservoir area (on the top) and 3-D image of the dam in the zoomed image (on the bottom).

2) Differential Interferometry on Multiple Satellite Images: Given the critical location of the dam area, to select the images, three different orbits were chosen and differential analysis was performed for terrain displacement detection using compatible products. For each pair of products, it has been necessary to verify the length of the perpendicular baseline and the subswath in which the structure was located. It is important to consider that SNAP allows to calculate from the unwrapped phase of the interferograms only the displacement of the terrain along the radar LOS, as already explained. In addition, the value provided by the "Phase to displacement" operator, made available by SNAP, is to be regarded as a relative value that needs to be corrected by choosing a reference point assumed as the fixed point, whose reference phase must be subtracted or added to the rest of the phase image. This operation should also be done using more than one reference point, as the phase tends to grow or decrease as it moves vertically along the image [50]. However, the dam is a structure that develops mainly in length and thus falling into a fairly uniform horizontal section of the image, where the phase variation can be considered limited to a single point of reference.

To find this reference, we chose the pixel with the highest value of coherence in the interferogram among those with the lowest deformation probability, according to the geotechnical characteristics of the areas and thanks to *in situ* monitoring. We assumed that this point (coherence value practically close to one) may be considered stable. It is worth noting that manual selection refers to this added supervised information.

Through the pixel coordinates, from the unwrapped image, the reference phase value is taken and a new image is generated through the "Band Maths" operator and the command: "Unw_phase-ref_pixel_phase," that uses the selected pixel phase value to normalize all the other pixels phase values. As regard the reference point indication, this is a point corresponding to the dam body (inside the white area of the green rectangle in Fig. 11 on the right). To calculate the vertical displacements, the "Band Math" operator is still used and another image, that contains all the vertical displacements obtained from the normalized unwrapped phase, is generated.

It is worth to underline that since the center frequency of the Sentinel-1 sensor is 5.405 GHz, corresponding to a wavelength of 0.055 m, shifts of the order of millimeters may be appreciated.

The displacements have been calculated with respect to the positions corresponding to the first three assestimeters along the crest of the dam for all the orbits. The position of the assestimeters is shown in Fig. 7. The obtained results have then been compared with the ground data.

Coming back to satellite data, the first orbit has provided three images of May 6th, May 18th, and May 30th, 2016. The second

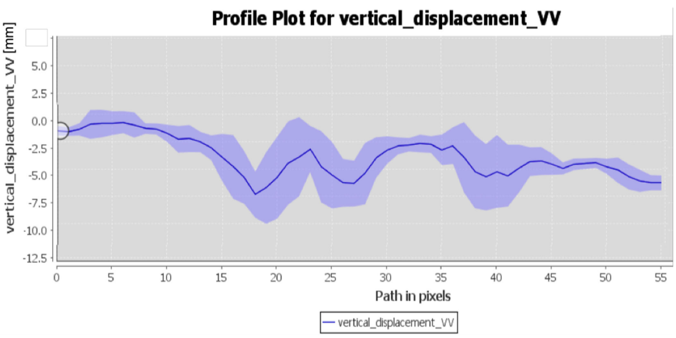

Fig. 14. Vertical displacements in mm over the path in pixels.

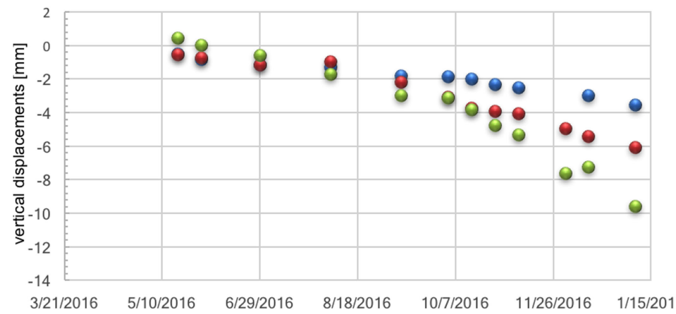

Fig. 15. Retrievals from interferograms on dam Sections: Section 5 in blue, Section 10 in red, and Section 13 in green.

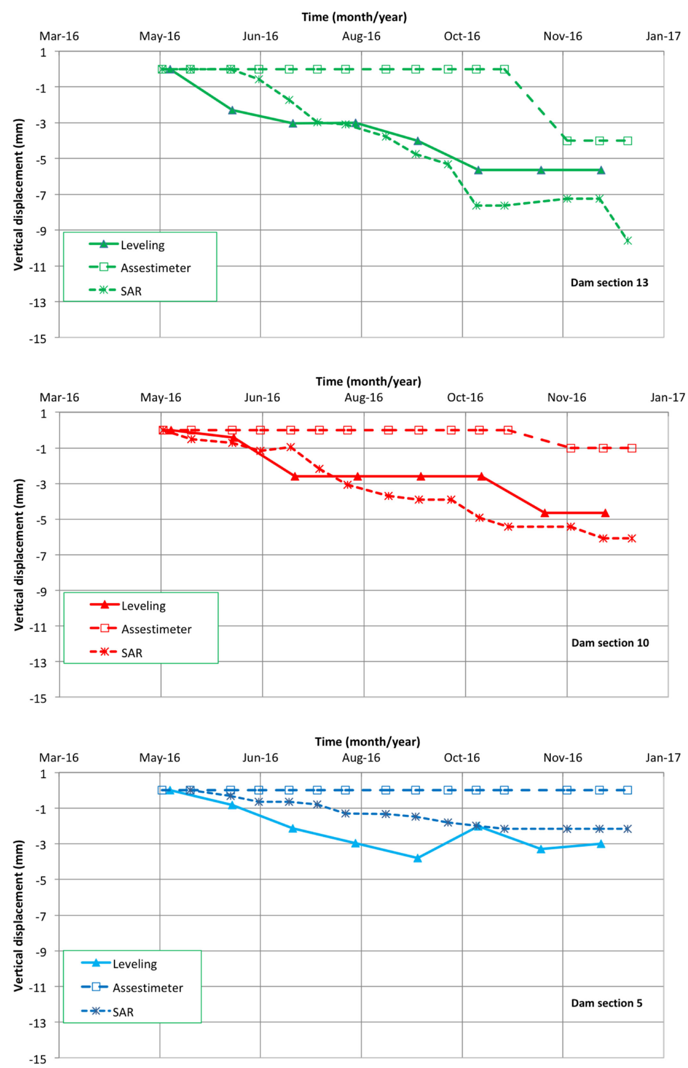

Fig. 16. Displacements from assestimeters and from high-precision leveling over the May 2016–January 2017 period compared to satellite interferometric measurements.

orbit has covered the month of June with only two acquisitions, corresponding to June 5th and June 29th, 2016. The third orbit has included acquisitions with greater time differences, covering the entire July to December period. However, some of these images pair cannot be used because their baseline was too low and the relative interferogram was practically useless, due to its high sensitivity to phase noise and atmospheric effects [27], [28]. For instance, this has been the case of the September 9th–21th couple and of the December 14th–26th couple. As a consequence, the results obtained by these pairs have not been taken into account in evaluating the overall trend of the structure movement.

For each displacement image, we can trace the “Profile Plot” of all the pixels belonging to a line that runs over the crest of the dam. From the profile graph extrapolated by the October 15th–27th, 2016 pair of the third orbit and shown in Fig. 14, it is shown that all the points of the crest have negative vertical displacements, which indicates a subsidence of the dam, even if all measurements are within a few millimeters.

It should be pointed out that Fig. 14 could help in detecting which dam zones are settling more than others in a fixed time interval. Conversely, as the assestimeters provide point-based information and typically only a few vertical lines of the embankment are equipped in this way, a comprehensive picture of the deformation mode of the dam embankment cannot be achieved by traditional monitoring. Furthermore, satellite data may suggest the dam Sections worth of attention, where traditional monitoring needs to be intensified.

From the profile graph, knowing the position of the pixels corresponding to the position of the *in situ* instrumentation, it is possible to extract the displacement of the single pixel. Retrievals are made near the assestimeter heads, at the reference cross Sections of the dam (Fig. 7), and are shown in Fig. 15. The figure shows that Section 5, close to assestimeter 1, has undergone lower displacements, while along Section 13, close to the assestimeter 3, embankment displacements are higher.

As the *in situ* data concern, assestimeter and high-precision leveling measurements are available from May 2009 up to the end of 2016. Ground data were zoomed on the period May 2016–December 2016, in order to make them consistent with the satellite interferometric retrievals. They are shown in Fig. 16 for the three reference cross Sections (5, 10, and 13) of the dam embankment. It is possible to notice that in this time interval dam displacements—as expected—are very small with the order of a few millimeters. It should be pointed out that since the dam had been built almost 30-years ago, consolidation of the foundation soils has reached its final stage and no appreciable settlements of the soil layers are therefore expected. In addition, in the considered reference period, the reservoir level was almost constant (maximum water level is in between 366- and 370-m a.s.l. for this dam), being the dam not yet used for hydroelectric scope. However, considering the high seismic hazard associated to the dam site, the correspondence between traditional ground measurements (the only available in common surveillance of large dams) and satellite data could be of paramount relevance to interpret possible diffuse deformation modes caused by future strong earthquakes. It is worth noting that after a severe seismic event, that might occur, dam accessibility may be obstructed by damage to road infrastructures so that ground monitoring could become difficult to be carried out for a long time after the mainshock.

From Fig. 16, it can be observed that SAR and high-precision leveling data denote an increasing trend in displacement evolution, while the assestimeters are less sensitive to highlight the above change with time. All ground data, however, corroborate the important finding obtained from SAR measurements, that is, from May 2016 to December 2016, Section 5 has undergone lower displacements (around 3 mm) compared to Section 13 (around 7 mm).

This is an outstanding result since the vertical displacements provided by the traditional monitoring (assestimeters or precise leveling) is limited to a few measurement points, while the satellite interferometric measurements are widespread, and thus they can highlight critical zones that the *in situ* instrumentation cannot. Moreover, the satellite interferometric application may help government agencies in charge of dam safety to make a cross check on data provided by dam owners after emergency caused by extreme events, such as earthquakes or floods.

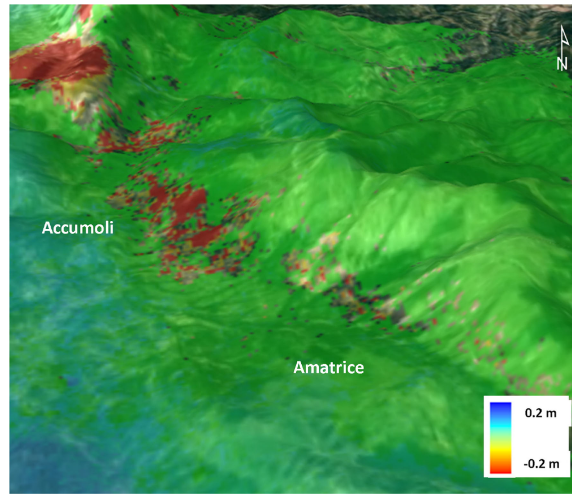

Fig. 17. Image of the displacements, related to August 24th earthquake—displacements up to 20 cm.

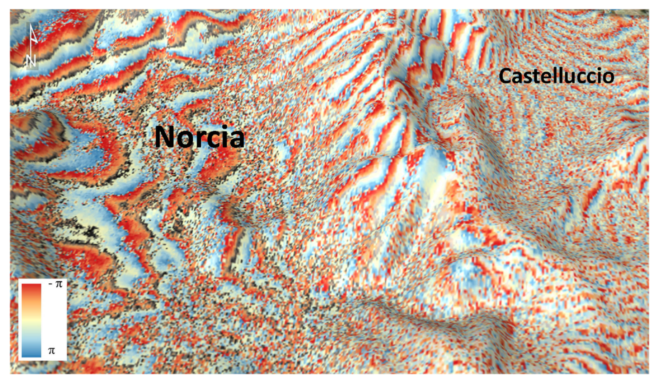

Fig. 18. Interferogram of October 30th earthquake with displacements up to 70 cm.

B. Campotosto Case Study

In the case of the Campotosto dam, it has not been possible to compare directly the satellite surveys with the *in situ* measurements, since ground data are not publicly available. For this reason, the following procedure has been performed: an interferometric analysis was carried out both with respect to the earthquake of August 24th and that of October 30th, 2016, for the entire area of interest, and then the obtained results were compared and validated with those calculated and published by the Italian National Institute of Geophysics and Vulcanology (INGV) and also with those presented by Cheloni in [51]. Such models are obtained both from satellite and on ground measurements.

To produce the interferograms, images from 21st August Sentinel-1A and 27th August Sentinel-1B have been selected for the earthquake of August 24th, 2016, and images from 26th October Sentinel-1B and 1st November Sentinel-1A have been selected for the earthquake of October 30th, 2016. Movements up to 20 cm in the first earthquake (Fig. 17) and up to 70 cm (Fig. 18) for the second in the areas of interest were detected. The results are completely in line with those found in [52] and in both INGV [53] and [54] for the events of the 24th August and 30th October, respectively, besides those found in [51], where the algorithms used are different. Specifically, in the latter case, many of the figures were made by using the Version 3.1 of the Generic Mapping Tools software [55], and different InSAR data acquired by different satellites (Sentinel-1, ALOS-2, and COSMO-SkyMed) were used for analysis.

In this paper, the first part of the analysis has been used to validate the procedure applied to SNAP for processing the Sentinel data. After that, to carry on the analysis of the Campotosto dam, the October 26th Sentinel-1B and the November 1st Sentinel-1A images, around the event of October 30th have been chosen because of higher coherence with respect to the others on the specific area of interest. The subswath 2 has then been chosen because it covered the entire reservoir.

The analysis has led to the results illustrated in the Figs. 19 and 20, where vertical movements of the area around the Campotosto dam and the map of displacements are shown.

It is noticed that the most affected dam is the Poggio Cancelli earth dam, the closest to the earthquake zone (on the left top of Fig. 20).

Vertical displacements between −13 and −18 cm are found near this dam. The other two have also significant displacements: smaller in the case of Sella Pedicate dam (about −8 cm), and large displacements for the Rio Fucino dam (about −15 cm). The latter case can be explained because this dam is built on a fault directly linked to that activated during the earthquake,

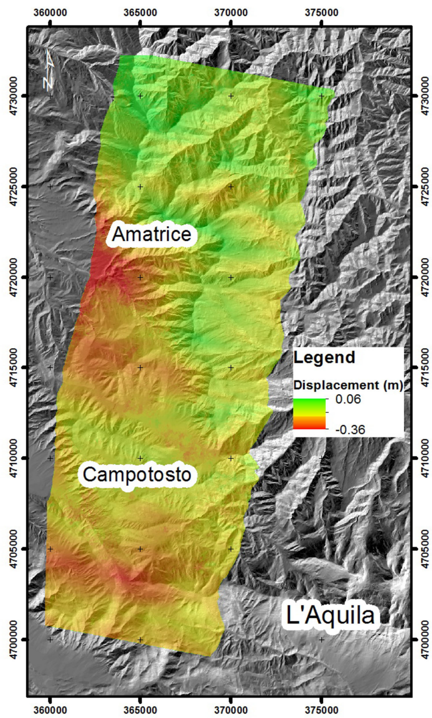

Fig. 19. Vertical movements of the area around the Campotosto dam.

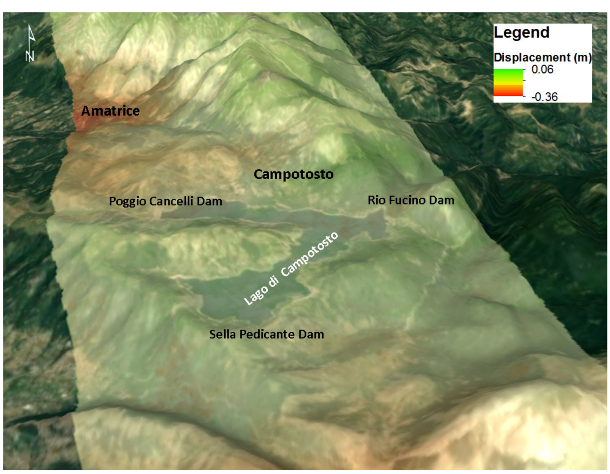

Fig. 20. Map of displacements.

although we have to say that images, available and retrieved in this case, had a lower coherence, therefore they were less reliable.

VI. Discussion and Conclusion

The usage of DInSAR in infrastructure monitoring is very promising, also for the availability of free data and tools, but the expected performance should still better assessed. In fact, even if the recent remote sensing literature proposes many approaches to the dam monitoring issue, only a few works provide validation analyses. This fact is mainly due to the lack of *in situ* measurements and to the necessity of interdisciplinary research teams to compare and interpret the data.

The aim of this paper has been to validate the application of DInSAR processing chain to dam monitoring, using open access data and free tools from the Copernicus programme. In particular, a DInSAR processing workflow has been proposed and discussed in detail.

To validate the proposed approach, the method has been applied to the case study of the Campolattaro dam, for which comparisons have been performed with *in situ* measurements, acquired by means of assestimeters and high-precision leveling. The comparison between satellite data and *in situ* measurements highlights the reliability of the developed interferometric procedure since the results reflect the general trend observed from ground instrument acquisitions. The developed methodology has later been applied also to the Campotosto reservoir, whose safety during the seismic sequence occurred in Central Italy in 2016 has caused huge concern in both dam owners and population placed downstream. In this latter case, data from ground instruments owned by the dam managers are still subject to confidentiality procedures. Therefore, the results obtained by the interferometric procedure were compared and validated with those published by INGV and by Cheloni in [55]. The unavailability of data even more convinced us of the importance of establishing immediate procedures that are quite easy to reproduce, such as those based on simple interferometric analysis. In fact, once these procedures have been completely settled and validated, we can be sure of having control and monitoring tools, which are independent of the on ground data management policies, with a view to putting the protection of human lives at the first place.

In general, the suggested approach is to use satellite data, available on wide areas, to integrate and improve ground data, which are instead limited to a few instrument locations, by optimizing time and costs. The exclusive use of remotely sensed data, however, sometimes becomes a necessary condition in scenarios where ground measurements cannot be performed, as for instance, in inaccessible sites, when catastrophic events have occurred. However, interferometric procedures need still to be assessed, in order to be fully reliable.

The results presented in this paper validate the proposed approach and encourage to adopt it when a fast and simple method of analysis is necessary, independent on ground data availability.

Furthermore, the possible implementation of different specific procedures for other case studies could increase the widespread of such monitoring technique. Indeed, on the basis of the reassuring results obtained in the different fields of applications, it is possible to emphasize the advantages that this technique has demonstrated.

1) Excellent cost-benefit ratio for wide area monitoring applications.
2) High precision (subcentimeter) in deformation assessment (comparable to the most advanced techniques like GPS).
3) Very high densities of monitored points (from hundreds to thousands of points per km^2).
4) Accuracy in target georeferencing (less than 5 m).

Finally, a further development of this paper could be the improvement of the overall coherence of SAR interferograms, as investigated in [56], [57]. Many of the unusable low-coherence images contain in fact specific information for the observation period and the area of interest, therefore their recovery and reuse would be of great importance for further analysis applications of the area.

Future work will also include the use of data from other Sentinels of the Copernicus Programme, such as the optical data of Sentinel-2 in order to enhance the overall information over a specific area.

ACKNOWLEDGMENT

The authors would like to thank the anonymous reviewers for their constructive criticism and valuable comments, undoubtedly of great help in improving our paper.

REFERENCES

[1] A. Di Pasquale, G. Nico, A. Pitullo, and G. Prezioso, "Monitoring strategies of earth dams by ground-based radar interferometry: How to extract useful information for seismic risk assessment," *Sensors*, vol. 18, 2018, Art. no. 244.

[2] S. Sica and L. Pagano, "Performance-based analysis of earth dams: Procedures and application to a sample case," *Soils Found.*, vol. 49, pp. 921–940, 2009.

[3] I. M. Idriss, J. M. Mathur, and H. B. Seed, "Earth dam foundation interaction during earthquakes," *Earthquake Eng. Struct. Dyn.*, vol. 2, no. 4, pp. 313–323, 1973.

[4] S. Sica, L. Pagano, and A. Modaressi, "Influence of past loading history on the seismic response of earth dams," *Comput. Geotech.*, vol. 35, pp. 61–85, 2008.

[5] T. E. Martin and E. C. McRoberts, "Some considerations in the stability analysis of upstream tailings dams," in *Proc. 6th Int. Conf. Tailings Mine Waste*, Fort Collins, Colorado, Jan. 1999, pp. 287–302.

[6] T. Wang, D. Perissin, F. Rocca, and M.-S. Liao, "Three Gorges dam stability monitoring with time-series InSAR image analysis," *Sci. China Earth Sci.*, vol. 54, no. 5, pp. 720–732, May 2011.

[7] D. Perissin, C. Prati, F. Rocca, and T. Wang, "PSInSAR analysis over the three gorges dam and urban areas in china," in *Proc. Joint Urban Remote Sens. Event*, May 2009, pp. 1–5.

[8] P. Milillo *et al.*, "Monitoring dam structural health from space: Insights from novel InSAR techniques and multi-parametric modeling applied to the Pertusillo dam Basilicata, Italy," *Int. J. Appl. Earth Observ. Geoinf.*, vol. 52, pp. 221–229, 2016.

[9] G. Grenerczy and U. Wegmuller, "Persistent scatterer interferometry analysis of the embankment failure of a red mud reservoir using ENVISAT ASAR data," *Natural Hazards*, vol. 59, pp. 1047–1053 2011.

[10] R. Toms *et al.*, "Monitoring an earthfill dam using differential SAR interferometry: La Pedrera dam, Alicante, Spain," *Eng. Geol.*, vol. 157, pp. 21–32, 2013.

[11] D. D. Martire *et al.*, "Comparison between Differential SAR interferometry and ground measurements data in the displacement monitoring of the earth-dam of Conza della Campania (Italy)," *Remote Sens. Environ.*, vol. 148, pp. 58–69, 2014.

[12] G. Nico, A. Di Pasquale, M. Corsetti, G. Di Nunzio, A. Pitullo, and P. Lollino, "Use of an advanced SAR monitoring technique to monitor old embankment dams," in *Engineering Geology for Society and Territory*, vol. 6, Cham, Switzerland: Springer, 2015, pp. 731–737.

[13] P. Milillo *et al.*, "Space geodetic monitoring of engineered structures: The ongoing destabilization of the Mosul dam, Iraq," *Sci. Rep.*, vol. 6, 2016, Art. no. 37408.

[14] J. Sousa *et al.*, "Potential of C-Band SAR interferometry for dam monitoring," *Procedia Comput. Sci.*, vol. 100, pp. 1103–1114, 2016.

[15] G. Lanzo *et al.*, "Reconnaissance of geotechnical aspects of the 2016 Central Italy earthquakes," *Bull. Earthq. Eng.*, pp. 1–38, 2018.

[16] A. D. Russo, S. Sica, S. D. Gaudio, R. D. Matteis, and A. Zollo, "Near-source effects on the ground motion occurred at the Conza dam site (Italy) during the 1980 Irpinia earthquake," *Bull. Earthq. Eng.*, vol. 15, no. 10, pp. 4009–4037, Oct. 2017.

[17] M. Crosetto, O. Monserrat, M. Cuevas-Gonzlez, N. Devanthry, and B. Crippa, "Persistent scatterer interferometry: A review," *ISPRS J. Photogrammetry Remote Sens.*, vol. 115, pp. 78–89, 2016. [Online]. Available: http://www.sciencedirect.com/science/article/pii/S0924271615002415

[18] P. Snoeij *et al.*, "The sentinel-1 radar mission: Status and performance," in *Proc. Int. Radar Conf. Surveillance Safer World*, Oct. 2009, pp. 1–6.

[19] European Commission, Copernicus Programmme Web Site. [Online]. Available: http://www.copernicus.eu/

[20] European Space Agency (ESA), Science Toolbox Exploitation Platform. [Online]. Available: http://step.esa.int/main/

[21] European Space Agency (ESA), Copernicus Scientific Data Hub. [Online]. Available: http://www.copernicus.eu/

[22] European Space Agency (ESA), Sentinel-1 User Handbook. [Online]. Available: https://sentinels.copernicus.eu/documents/247904/685163/Sentinel-1_User _Handbook

[23] A. K. Gabriel, R. M. Goldstein, and H. A. Zebker, "Foundation instrumentation," *J. Geophys. Res.*, vol. 94, pp. 9183–9191, 1989.

[24] D. Massonnet *et al.*, "The displacement field of the Landers earthquake mapped by Radar Interferometry," *Nature*, vol. 364, pp. 138–142, 1993.

[25] Z. M. Panozzo, "SAR image quality assesment," *Master in Emergency Early Warning and Response Space Applications.* Còrdoba, Argentina: Universidad Nacional de Còrdoba, 2012. [Online]. Available: http://aulavirtual.ig.conae.gov.ar/moodle/pluginfile.php/513/mod_page/content/28/MirkoPanozzoZenere.pdf

[26] A. Ferretti, A. Monti-Guarnieri, C. Prati, and F. Rocca, "Insar principles: Guidelines for SAR interferometry processing and interpolation," ESA Publications TM-19, ESA, Frascati, Italy, 2007.

[27] A. Ferretti, A. Monti-Guarnieri, C. Prati, F. Rocca, and D. Massonnet, *InSAR Principles: Guidelines for SAR Interferometry Processing and Interpretation*. Postbus 229, 2200 AG Noordwijk: ESA Publications, 2007.

[28] P. A. Rosen *et al.*, "Synthetic aperture radar interferometry," *Proc. IEEE*, vol. 88, no. 3, pp. 333–382, Mar. 2000.

[29] T. Toutin and L. Gray, "State-of-the-art of elevation extraction from satellite SAR data," *ISPRS J. Photogrammetry Remote Sens.*, vol. 55, no. 1, pp. 13–33, 2000.

[30] C. L. Werner, U. Wegmuller, and T. Strozzi, "Processing strategies for phase unwrapping for InSAR applications," in *Proc. 4th Eur. Conf. Synthetic Aperture Radar*, vol. 1, 2002, pp. 353–356. [Online]. Available: https://www.gamma-rs.ch/uploads/media/2002-4_PhaseUnwrapping.pdf

[31] European Space Agency, "Sentinel Application Platform (SNAP) Website," 2017. [Online]. Available: http://step.esa.int/main/toolboxes/snap/

[32] Stanford University, "Statistical-cost, Network-flow Algorithm for Phase Unwrapping (SNAPHU) Website," 2017. [Online]. Available: http://nova.stanford.edu/sar_group/snaphu/

[33] C. W. Chen and H. A. Zebker, "Network approaches to two-dimensional phase unwrapping: Intractability and two new algorithms," *J. Opt. Soc. Amer. A*, vol. 17, no. 3, pp. 401–414, 2000.

[34] C. W. Chen and H. A. Zebker, "Two-dimensional phase unwrapping with use of statistical models for cost functions in nonlinear optimization," *J. Opt. Soc. Amer. A*, vol. 18, no. 2, pp. 338–351, 2001. [Online]. Available: http://josaa.osa.org/abstract.cfm?URI=josaa-18-2-338

[35] C. W. Chen and H. A. Zebker, "Phase unwrapping for large SAR interferograms: Statistical segmentation and generalized network models," *IEEE Trans. Geosci. Remote Sens.*, vol. 40, no. 8, pp. 1709–1719, Aug. 2002.

[36] H. Yu, Z. Li, and Z. Bao, "Residues cluster-based segmentation and outlier-detection method for large-scale phase unwrapping," *IEEE Trans. Image Process.*, vol. 20, no. 10, pp. 2865–2875, Oct. 2011.

[37] D. Small and A. Schubert, "Guide to ASAR Geocoding," 2008. [Online]. Available: http://www.geo.uzh.ch/microsite/rsl-documents/research/publications/other-sci-communications/2008_RSL-ASAR-GC-AD-v101–0335607552/2008_RSL-ASAR-GC-AD- v101.pdf

[38] J. P. Stewart *et al.*, "Engineering reconnaissance following the 2016 M 6.0 central Italy earthquake: Ver. 2," *Geotechnical Extreme Events Reconnaissance Association*, Report No. GEER - 050A, Sep. 2016. [Online]. Available: http://www.geerassociation.org/

[39] Agenzia Sannita Energia Ambiente (ASEA), Official Website. [Online]. Available: http://www.aseaenergia.eu/la-diga-di-campolattaro?lang=en

[40] F. Galadini and P. Galli, "Paleoseismology of silent faults in the central Appennines (Italy): The Mt. Vettore and Laga Mts. faults," *Ann. Geophys.*, vol. 46, no. 5, pp. 815–836, 2003.

[41] R. Lanari *et al.*, "Surface displacements associated with the L'Aquila 2009 M_w 6.3 earthquake (central Italy): New evidence from SBAS-DInSAR time series analysis," *Geophys. Res. Lett.*, vol. 37, 2010, Art. no. L20309.

[42] D. Infante, "Il monitoraggio di sbarramenti idraulici mediante l'uso di immagini satellitari elaborate con tecnica DInSAR," Masters' Thesis, Dipartimento di Ingegneria civile-edile-ambientale, Università degli studi di Napoli Federico II, Napoli, Italy, 2012/2013.

[43] F. Gatelli, A. Monti Guarnieri, F. Parizzi, P. Pasquali, C. Prati, and F. Rocca, "The wavenumber shift in SAR interferometry," *IEEE Trans. Geosci. Remote Sens.*, vol. 32, no. 4, pp. 855–865, Jul. 1994.

[44] E. Rodriguez and J. M. Martin, "Theory and design of interferometric synthetic aperture radars," *IEE Proc.-F*, vol. 139, no. 2, pp. 147–159, Apr. 1992.
[45] H. Zebker and J. Villasenor, "Decorrelation in interferometric radar echoes," *IEEE Trans. Geosci. Remote Sens.*, vol. 30, no. 5, pp. 950–959, Sep. 1992.
[46] R. Hanssen, "Assessment of the role of atmospheric heterogeneities in ERS tandem SAR interferometry," Delft Univ. Press, Delft, the Netherlands, DEOS Rep. 12698.1, 1998.
[47] R. M. Goldstein and C. L. Werner, "Radar interferogram filtering for geophysical applications," *Geophys. Res. Lett.*, vol. 25, no. 21, pp. 4035–4038, 1998.
[48] A. Barra *et al.*, "A methodology to detect and update active deformation areas based on sentinel-1 SAR images," *Remote Sens.*, vol. 9, no. 10, 2017, Art. no. 1002. [Online]. Available: http://www.mdpi.com/2072-4292/9/10/1002
[49] A. Minchella and P. Marinkovic, "Example of a full processing for DEM generation using NEST," ESA, Frascati, Italy, 2012. [Online]. Available: https://earth.esa.int/documents/507513/1077939/NEST_ERS-ETNA_DEM_091020 12.pdf
[50] M. Crosetto, O. Monserrat, M. CuevasGonzàlez, N. Devanthéry, and B. Crippa, "Persistent scatterer interferometry: A review," *ISPRS J. Photogrammetry Remote Sens.*, vol. 115, pp. 78–89, 2016.
[51] D. Cheloni *et al.*, "Geodetic model of the 2016 Central Italy earthquake sequence inferred from InSAR and GPS measurements," in *Proc. EGU General Assem. Conf. Abstr.*, vol. 19, Apr. 2017, paper 9191. [Online]. Available: http://adsabs.harvard.edu/abs/2017EGUGA..19.9191C
[52] "Gruppo di Lavoro INGV sul Terremoto in centro Italia. Relazione sullo stato delle conoscenze della sequenza sismica in centro Italia 2016–2017," Tech. Rep., Feb. 2017, doi: 10.5281/zenodo.267984.
[53] INGV, "Measurements of soil displacement through satellite interferometry," Tech. Rep., Sep. 2016. [Online]. Available: https://ingvterremoti.wordpress.com/2016/09/16/terremoto-in-italia-centrale-misure-dello-spostamento-del-suolo-tramite-interferometria-satellitare/
[54] INGV, "Differential Interferogram obtained from European Sentinel-1 satellite radar data," Tech. Rep., Nov. 2016. [Online]. Available: https://ingvterremoti.wordpress.com/2016/11/02/prime-interpretazioni-dallinterferogramma-differenziale-ottenuto-da-dati-radar-del-satellite-europeo-sentinel-1/?blogsub=confirming#subscribe-blog
[55] P. Wessel and W. Smith, "New improved version of the Generic Mapping Tools (GMT) released," *EOS Earth Space Sci. News*, vol. 79, no. 47, pp. 579–579, 1998.
[56] A. Borzì, M. D. Bisceglie, C. Galdi, L. Pallotta, and S. L. Ullo, "Phase retrieval in SAR interferograms using diffusion and inpainting," in *Proc. IEEE Int. Geosci. Remote Sens. Symp.*, Jul. 2010, pp. 2912–2915.
[57] S. L. Ullo, M. D. Bisceglie, and C. Galdi, "A new algorithm for noise reduction and quality improvement in SAR interferograms using inpainting and diffusion," in *Proc. IEEE Int. Geosci. Remote Sens. Symp.*, Jul. 2011, pp. 3602–3605.

Silvia Liberata Ullo (SM'18), received the *cum laude* degree in electronic engineering from Federico II University, Naples, Italy, in 1989.

She worked with Italtel s.p.a. for eight years as a Research Engineer and Production Manager, and for four years with the Benevento Municipality, as an Officer at the Data Elaboration Center. She was a member of the Board of Directors for the Municipal Transport Society, Benevento, Italy for three years (1994–1997). Since 2004, she has been a Researcher with University of Sannio, Benevento, Italy with interests in data analysis through satellite remote sensing for earth observation, communication networks with particular reference to the sensors networks and smart grids, radar detection in non-Gaussian environment, non-Gaussian models for the backscatter signal from natural surfaces. She is an author of several scientific papers. Full list is available at https://www.ding.unisannio.it/persone/docenti/ullo#pubblicazioni. She was the recipient of the Italtel scholarship, accomplished a Microeconomics Program at Harvard University, in August 1990, and the Master of Science in Management at Massachusetts Institute of Technology, Cambridge, MA, USA in 1992.

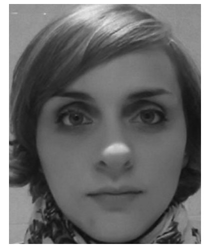

Pia Addabbo received the B.Sc. and M.Sc. degrees in telecommunication engineering, and the Ph.D. degree in information engineering from the Universit degli Studi del Sannio, Benevento, Italy, in 2005, 2008, and 2012, respectively.

She is a Researcher at the "Giustino Fortunato" University, Benevento, Italy. Her research interests include statistical signal processing applied to radar target recognition, global navigation satellite system reflectometry, and hyperspectral unmixing.

Dr. Addabbo is a member of IEEE from 2009 and coauthor of scientific publications in international journals and conferences.

Diego Di Martire received the master's degree in environmental engineering from the University of Naples, Federico II, Italy, in 2003, and the Ph.D. degree in environmental systems analysis from the University of Naples, Federico II, Italy, in 2013. He is a Researcher with the Department of Earth Sciences, Environment and Resources, Federico II University of Napoli, Napoli, Italy. He has ten years of research experience on the prediction and prevention of high-risk slope movements and the geothecnical validation of satellite interferometric data. In particular, his principal fields of investigation regard the development of landslide hazard and risk assessment techniques (statistical and physically based models) based on geological and geotechnical characterization, monitoring, and modeling; processing and interpretation of satellite interferometric data for landslides, structures and infrastructures monitoring studies by their integration with the ground-based measurements and numerical modeling.

Stefania Sica received the *cum laude* degree in civil engineering from the University of Naples Federico II, Napoli, Italy, in 1997, and the Ph.D. degree in geotechnical engineering from the University Consortium of Roma La Sapienza and Napoli Federico II, Napoli, Italy, in 2001.

From June 2001 to December 2004, she was a Scientist Assistant with the Department of Geotechnical Engineering, University of Naples, Napoli, Italy. From November 2006 to October 2017, she was an Assistant Professor with the University of Sannio, Benevento, Italy. Since November 2017, she has been an Associate Professor with the University of Sannio, Benevento. She spent some training periods abroad in different universities and research centers and participated to several national and international research projects. She has authored and coauthored more than 130 scientific papers published on peer-reviewed international journals, national journals, and proceedings of national and international conferences and symposia. Her research interests include the theoretical and numerical analysis of different geotechnical structures (earth dams, deep, and shallow foundations) under static and seismic conditions; soil-structure interaction problems for historical buildings and bridges; site response analysis for microzonation studies.

Prof. Sica is a member of the Earthquake Geotechnical Engineering Committee of the Italian Geotechnical Society. She collaborated to the supporting activity of AGI to the Department of Civil Protection in the emergency after the LAquila earthquake in 2009 and the Emilia earthquake of 2012. She is a Reviewer for different international journals.

Nicomino Fiscante was born in Benevento, Italy, on January 26, 1982. He received the M.Sc. degree (*cum laude*) in telecommunication engineering from the University of Sannio, Benevento, Italy, in 2007.

From January to June 2007, he was a trainee with the Antenna Group, Netherlands Organization for Applied Scientific Research (TNO Defense, Security, and Safety), The Hague, The Netherlands. From 2008 to 2012, he was with Mediterranean Agency for Remote Sensing and Environmental Control, Benevento, Italy. From 2012 to 2014, he was with Advanced Research Technology Spa, Passignano sul Trasimeno, Italy. Since 2014, he has been a Project Manager with Geoslab (now GeneGIS GI) and has increased numerous work experience both nationally and internationally, thanks to the collaboration with important Companies, Research Centers, Universities and Institutions. His research interests include remote sensing, GIS, data processing, TLC and EM systems, mobile mapping systems, and renewable resources.

Luca Cicala received the Ph.D. degree in electronic and telecommunications engineering from the University of Naples Federico II, Napoli, Italy, in 2008.

Since 2005, he has been a System Engineer and Researcher with the Italian Aerospace Research Center, Italy where, currently, he also leads research and technology development projects. He mainly designs image processing technologies and systems, in particular for Intelligence, Surveillance and Reconnaissance and Remote Sensing applications. In these fields, he also investigated the integration of aerial or satellite images with other data sources, in particular navigation sensors and geographical databases, proposing novel approaches and solutions. His research interests include focused both methods and applications.

Cesario Vincenzo Angelino received the Ph.D. degree in automation and signal and image processing, and electronic and telecommunications engineering, respectively, from the University of Nice-Sophia Antipolis, Nice, France and the University of Naples Federico II, Napoli, Italy, in 2011.

During his Ph.D., the research activity was in the field of statistical image processing, with attention to digital photography and remote-sensing applications. In 2011, he joined the Italian Aerospace Research Center, Capua, Italy where he is currently a researcher. His research interest includes computer vision and image processing for Environmental Remote Sensing and for Intelligence, Surveillance and Reconnaissance Missions, with focus on aspects such as video and imagery processing, sensor fusion among cameras and navigation sensors, environmental application of remote sensing from satellites and unmanned aerial vehicles.